Figure S1

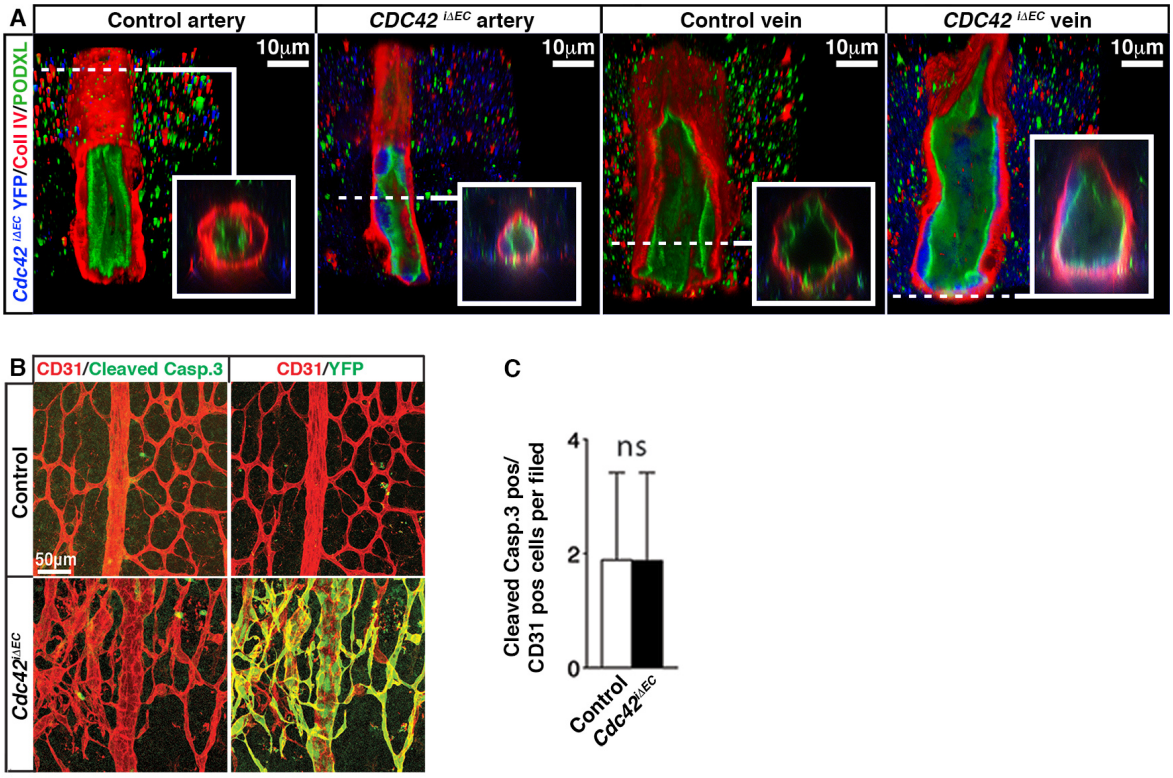

Figure S1: Loss of Cdc42 does not compromise endothelial apical-basal polarity nor EC survival during postnatal retinal development (A) 3-D reconstructions and optical sections of arteries and veins from P7 control and *Cdc42*$^{i\Delta EC}$ retinas. Dashed lines indicate the location of the cross-sectional view shown in the boxed areas. Podocalyxin (PODXL) (green) marks the apical (luminal) surface of blood vessels, while Coll IV stains the basal (abluminal) surface. Note that apical-basal polarization of blood vessels in *Cdc42*$^{i\Delta EC}$retinas appears normal and that YFP+ (*Cdc42*KO-EC) cells (blue) are properly located between the apical and basal domains. **(B)** Analysis of EC apoptosis in P7 control and *Cdc42*$^{i\Delta EC}$ retinas stained for ECs (CD31) and apoptosis (cleaved caspase-3). **(C)** Quantification of apoptotic ECs in the retina vasculature (control n=18 fields; *Cdc42*$^{i\Delta EC}$ n=18 fields from 2 animals per group from 2 independent litters). Graph shows mean ± s.d (Unpaired two-tailed t-test, ns – non significant).

Figure S2

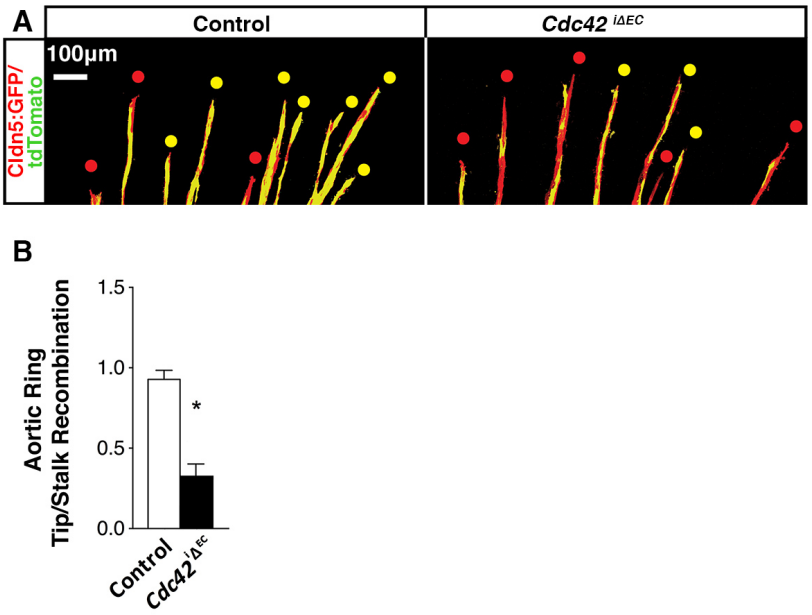

Figure S2: Cdc42 is required for endothelial tip selection in aortic rings cultures

(A) Confocal images of aortic ring sprouts from control and *Cdc42*$^{i\Delta EC}$ mice. Cldn5:GFP expression labels all ECs (red); recombined ECs labeled by tdTomato (green). Based on tdTomato expression we calculated the recombination rate to be 90±0.04%. Red dots denote non-recombined tip cells and yellow dots recombined tip cells. **(B)** Quantification of tip/stalk cell recombination in aortic rings from control (n=8) and *Cdc42*$^{i\Delta EC}$ (n=12) animals (at least 225 sprouts were analyzed per group). Graph shows mean ± s.d (Unpaired two-tailed t-test; * $p \leq 0.01$).

Figure S3

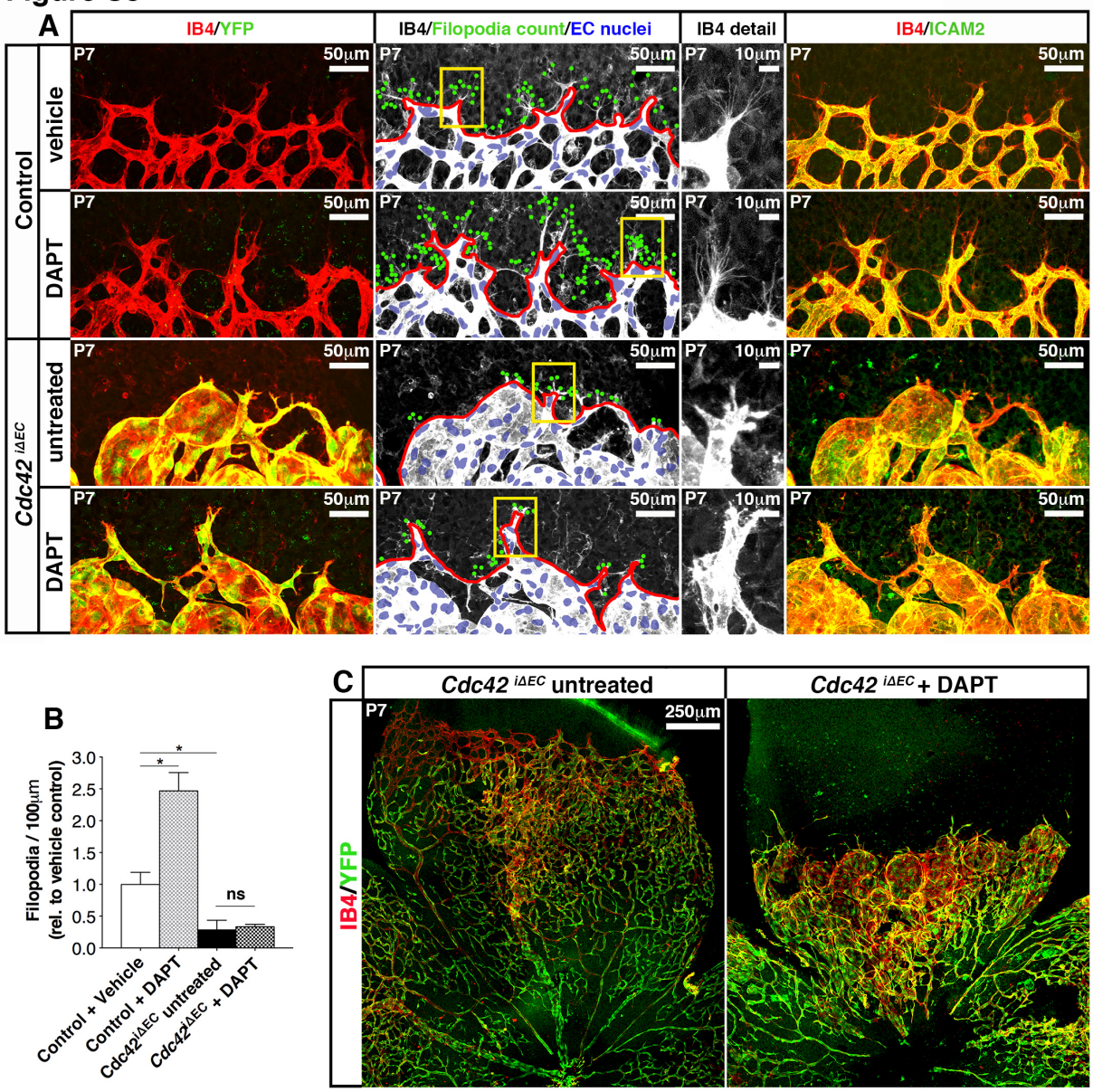

Figure S3: Pharmacological inhibition of Notch signaling fails to induce filopodia formation in *Cdc42*$^{i\Delta EC}$ retinas but aggravates vascular malformations

(A) Confocal images of P7 control and *Cdc42*$^{i\Delta EC}$ retinas (untreated, vehicle treated or treated with the γ-secretase inhibitor DAPT for 12hours). EC are labeled with IB4, recombinant cells by YFP and vascular lumens by ICAM2. Single filopodia are indicated by green dots and the position of EC nuclei are indicated based on ERG staining. Red lines delineate the vascular front length. Yellow boxes indicate tip cells shown in higher resolution to the right. Note that DAPT induces filopodia formation (green dots) in the control group but not in *Cdc42*$^{i\Delta EC}$ retinas. **(B)** Quantification of filopodia per 100µm vascular front; Control+Vehicle (n=3); Control+DAPT (n=4); *Cdc42*$^{i\Delta EC}$ untreated (n=9); *Cdc42*$^{i\Delta EC}$+DAPT (n=3); values indicate mean±s.d. Between 65 and 120 tip cells were analyzed per group. Graph shows mean ±

s.d (Unpaired two-tailed t-test, ns – non significant; * p≤0.05). **(C)** Overview confocal images showing vascular malformation in DAPT treated and untreated P7 *Cdc42*^{iAEC} retinas. Note how DAPT treatment aggravates the vascular malformations.

Figure S4

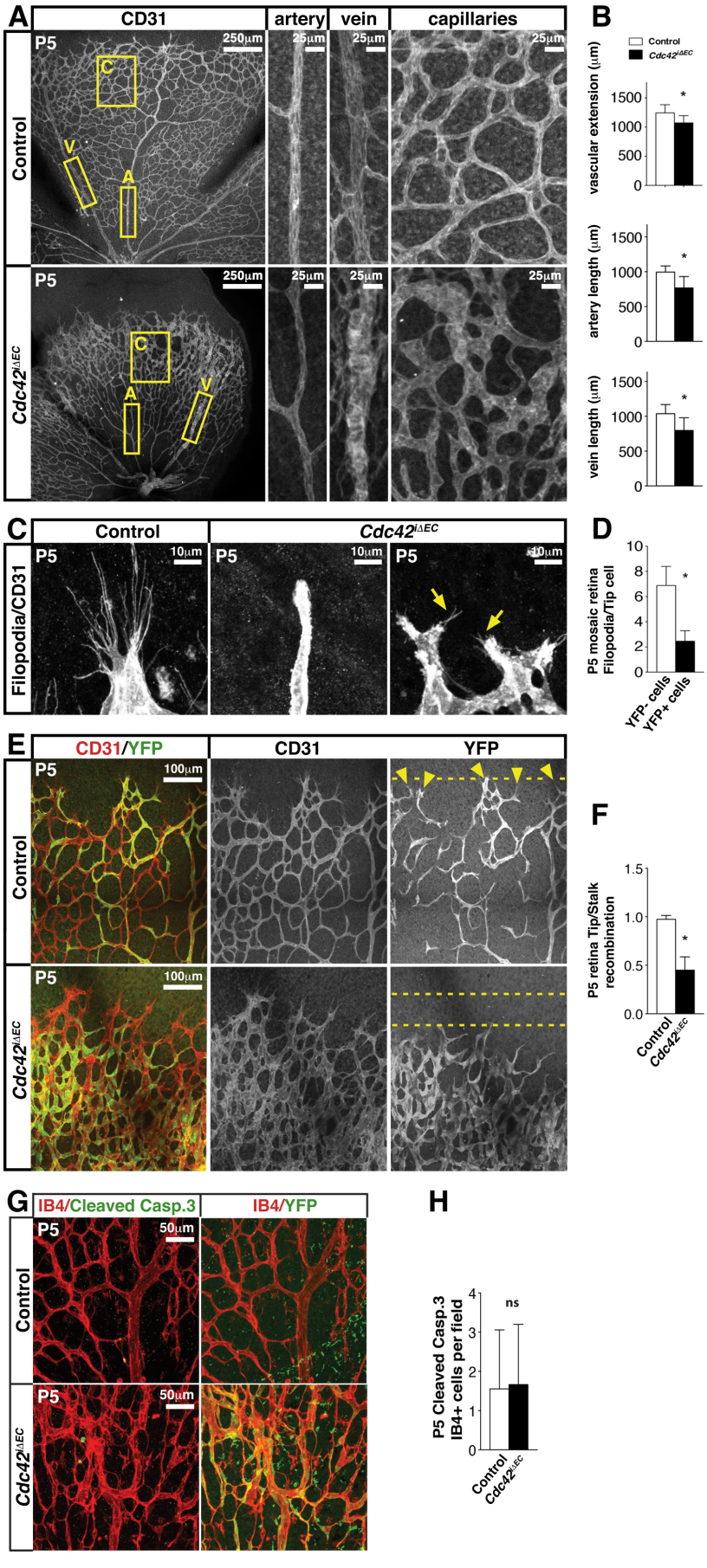

Figure S4: Vascular phenotypes in P5 *Cdc42*$^{i\Delta EC}$ retinas

(A) P5 retinal whole-mounts stained with CD31 to visualized blood vessels. Note the reduced vascular expansion towards the retinal periphery and vascular malformations in veins (V) and capillaries (C), but not in arteries (A) of *Cdc42*$^{i\Delta EC}$ retinas. Right panels: high-magnification images of boxed areas reveal tortuous dilations in vein and capillaries, and protuberant endothelial structures in *Cdc42*$^{i\Delta EC}$ retinas. **(B)** Quantification of vascular extension and of arterial and venous length in P5 control (n=7) and *Cdc42*$^{i\Delta EC}$ retinas (n=5); *p<0.05. **(C)** ECs in the tip cell position from control and highly recombined (>80%) *Cdc42*$^{i\Delta EC}$ P5 retinas labeled with CD31. Note that *Cdc42*KO-EC at tip cell positions are morphologically abnormal and had a significant decrease in number of filopodia (indicated by yellow arrows). **(D)** Quantification of filopodia number per tip cell in highly recombined P5 *Cdc42*$^{i\Delta EC}$ (n=3) retinas; more than 125 tip cells were analyzed; *p<0.05. (E) Images of sprouting front areas showing the distribution of recombinant cells (YFP+) in P5 control and

Cdc42$^{i\Delta EC}$ retinas stained for ECs (CD31) and YFP. Yellow arrowheads indicate recombinant endothelial tip cells (YFP+) and yellow dashed lines mark vascular areas where no recombinant cells are found. **(F)** Quantification of TR/SR ratios in P5 control (n=5) and *Cdc42*$^{i\Delta EC}$ (n=5) retinas showing a disadvantage of *Cdc42*KO-EC to be in the tip cell position as shown in P7 retinas;
*p<0.05. **(G)** Analysis of EC apoptosis in P5 control and *Cdc42*$^{i\Delta EC}$ retinas stained for ECs (IB4) and apoptosis (cleaved caspase-3). **(H)** Quantification of apoptotic ECs in the retina vasculature (control n=2 and *Cdc42*$^{i\Delta EC}$ n=3 from 2 independent litters). Graphs show mean ± s.d (Unpaired two-tailed t-test, ns – non significant; * p≤0.05).

Figure S5

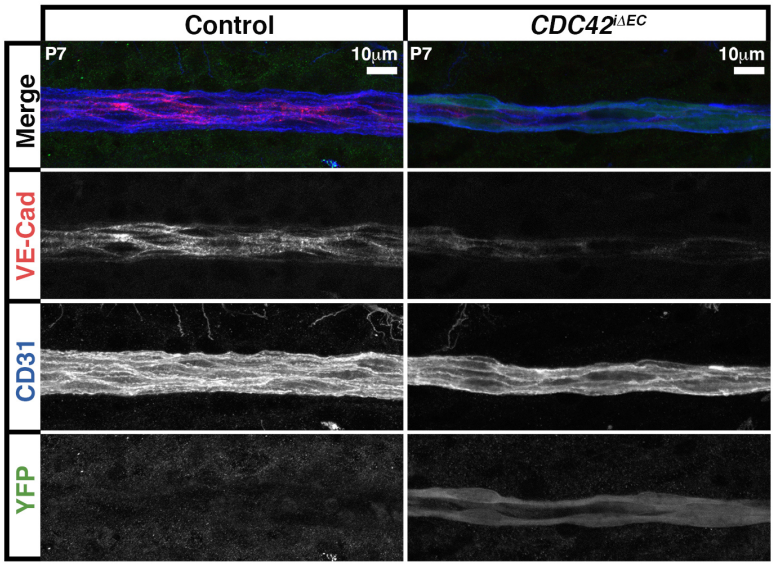

Figure S5: Effects on EC junctions in *Cdc42*$^{\Delta EC}$ arteries.

Confocal images of highly recombined arteries from control and *Cdc42*$^{\Delta EC}$ retinas at P7, stained for YFP (green, to visualize recombination efficiency), VE-Cadherin (red) and CD31 (blue). Note that Cdc42 deficiency leads to disturbed VE-Cadherin localization at arterial EC junctions *in vivo* but that overall arterial morphology is not severely affected.

Figure S6

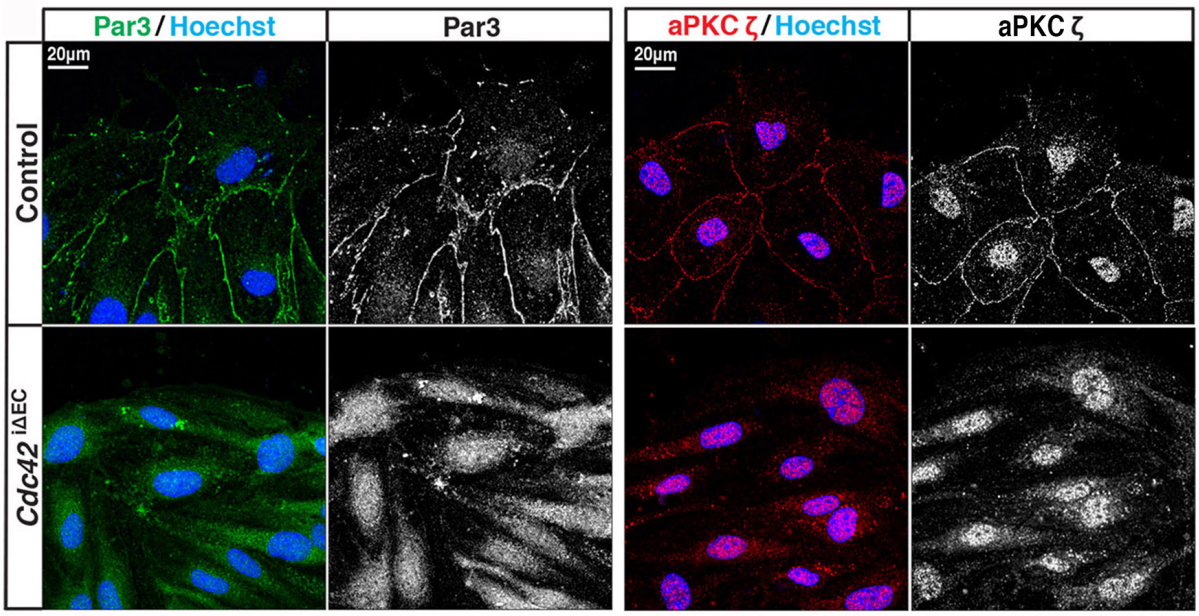

Figure S6: Cellular localization of Par complex proteins

Confocal images of primary brain ECs isolated from P7 control and *Cdc42*^{iΔEC} animals stained for Par3, atypical Protein Kinase C (aPKCζ) and Hoechst. Note that the membrane associated localization of Par3, and aPKCζ is lost in the absence of Cdc42.

Figure S7

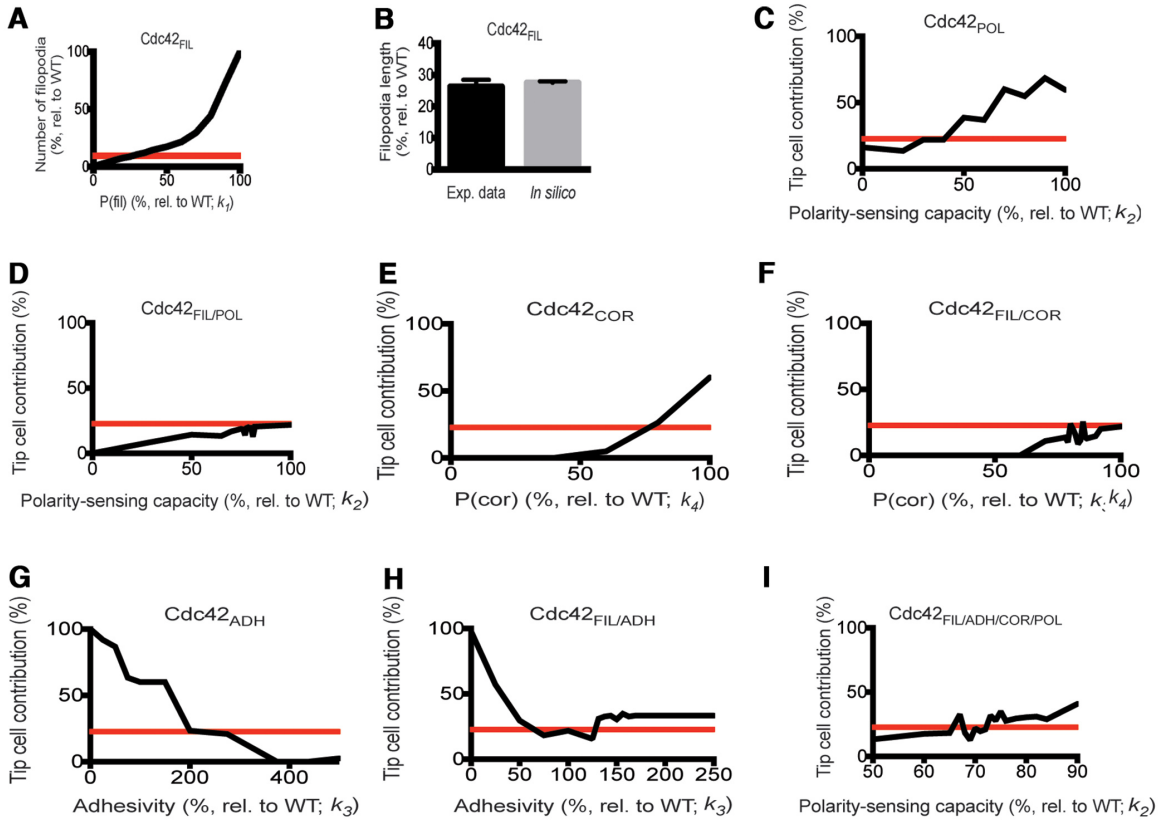

Figure S7: Computational modeling of the different Cdc42 driven cellular processes impacting on sprouting

(A) Sensitivity analysis of $Cdc42_{FIL}$ depicting dependence of filopodia number on the probability to extend filopodia in MSM-CPM (P(fil)). The red line indicates the experimentally observed reduction in filopodia number. **(B)** Filopodia length quantification (% relative to WT) in our experimental data (Exp. data) and *in silico* using the $Cdc42_{FIL}$ model. **(C-I)** Sensitivity analyses showing how the *Cdc42*KO cell contribution to the tip in simulated 6:4 *Cdc42*KO:WT sprouts changes when **(C)** polarity-sensing capacity ($Cdc42_{POL}$), **(E)** the probability of extending junctional cortex protrusions ($Cdc42_{COR}$) and **(G)** intercellular adhesion ($Cdc42_{ADH}$) are modified independently or in combination **(D, F, H, I)**. The red line indicates the experimentally observed *Cdc42*KO cell contribution to the tip for 6:4 *Cdc42*KO:WT sprouts.

Figure S8

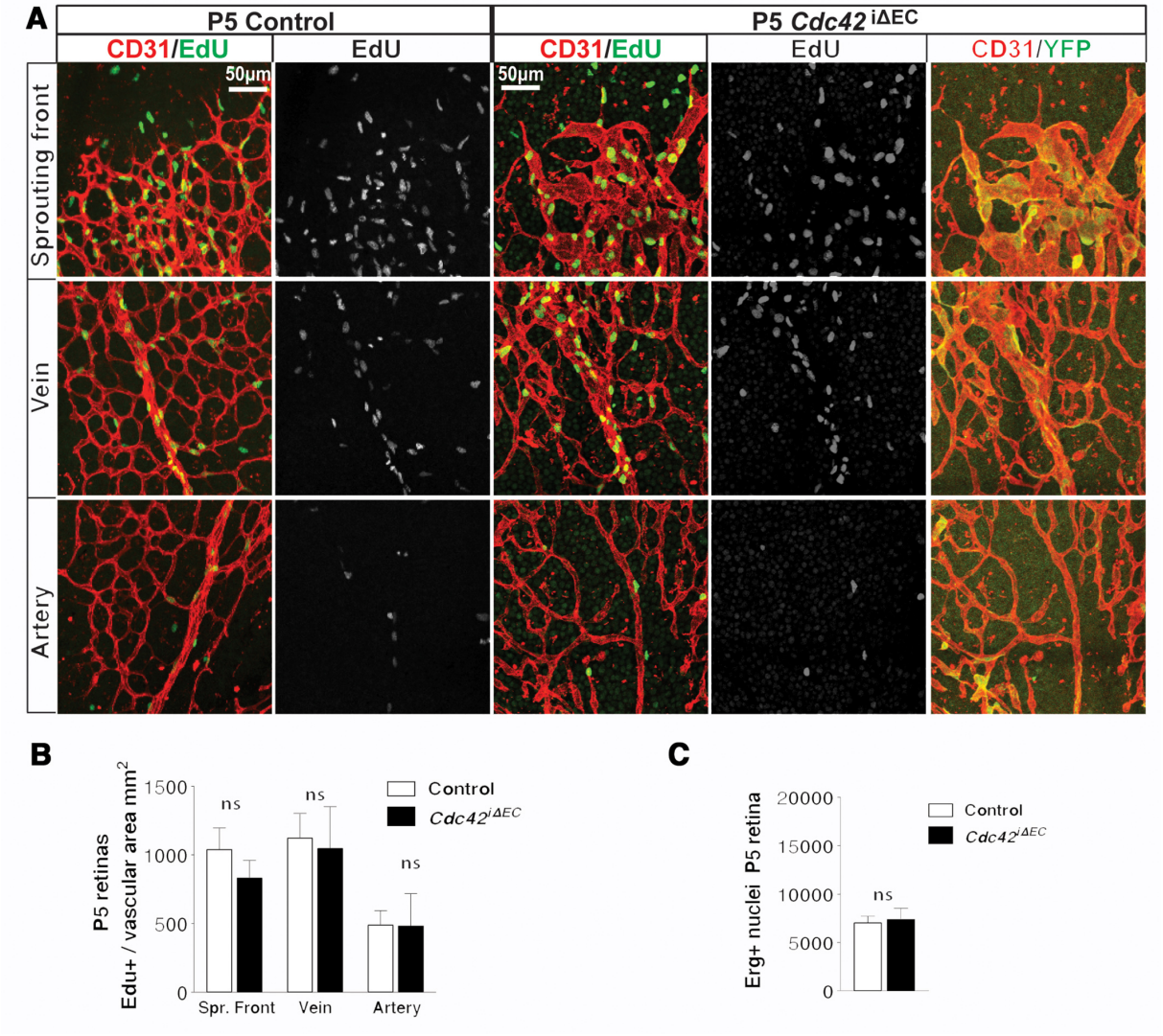

Figure S8: EC proliferation is not altered in P5 retinas

Analysis of EC proliferation in the sprouting front, veins and arteries of control and *Cdc42*$^{i\Delta EC}$ retinas. **(A)** Confocal images from P5 control and *Cdc42*$^{i\Delta EC}$ retina stained for ECs (CD31), proliferating cells (EdU), and recombination efficiency (YFP). **(B)** Quantification of EC proliferation in P5 retinas displayed as proliferating (EdU +) cells per vascular area in control (n=4) and *Cdc42*$^{i\Delta EC}$ (n=5) **(C)** Total number of ECs (ERG +) in control (n=3) and *Cdc42*$^{i\Delta EC}$ (n=4) retinas at P5. Graph shows mean ± s.d (Unpaired two-tailed t-test, ns – non significant)

Table S1

A

Wound assay	N° wounds analysed	1st row N° cells analysed	1st row % Polarized ECs	2nd row N° cells analysed	2nd row % Polarized ECs	3rd row N° cells analysed	3rd row % Polarized ECs
5h Control	8	205	**77.7**	61	**74.7**	65	**59.9**
5h Cdc42 $^{i\Delta EC}$	11	297	**38.7**	123	**36.2**	119	**35.3**
24h Control	10	554	**80.0**	145	**78.7**	151	**76.3**
24h Cdc42 $^{i\Delta EC}$	8	526	**38.3**	78	**33.9**	74	**34.9**

B

P7 Retina	Artery N° Cells analysed	Artery % Polarized ECs	Vein N° Cells analysed	Vein % Polarized ECs	Capillaries at sprouting front N° Cells analysed	Capillaries at sprouting front % Polarized ECs at -180°C	Capillaries at sprouting front % Polarized ECs at 0°
Control	120	**98.3**	219	**87.2**	361	**39.85**	**39.88**
Cdc42 $^{i\Delta EC}$	125	**97.6**	389	**46.0**	332	**18.74**	**35.74**

Table S1: Quantitative analysis of EC axial polarity

Detailed quantitative analysis of EC axial polarity in **(A)** scratch wound assay performed with primary brain ECs isolated from P7 control and *Cdc42*$^{i\Delta EC}$ mice, 5h (Control n=8; *Cdc42*$^{i\Delta EC}$ n=11) and 24h (Control n=10; *Cdc42*$^{i\Delta EC}$ n=8) post scratch in the 1st, 2nd and 3th cell row and **(B)** arteries (n=3), veins (n=3) and capillaries at the sprouting front (n=6) from P7 control and *Cdc42*$^{i\Delta EC}$ retinas. See material and methods section and Fig. 5 and 6 for more information about quantification method used in this analysis.

Movies

Cdc42 is dispensable for endothelial lumen formation in the postnatal retina

Movie 1

Movie 2

Movie 3

Movie 4

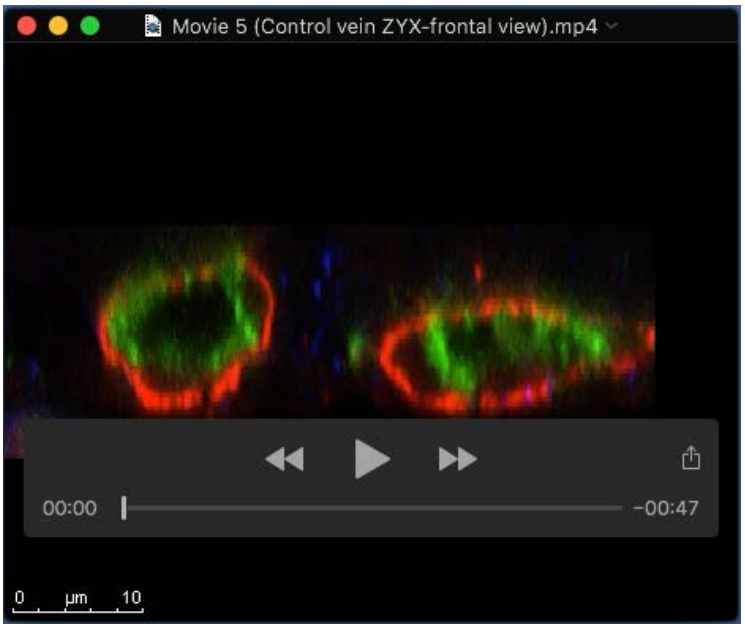

Movie 5

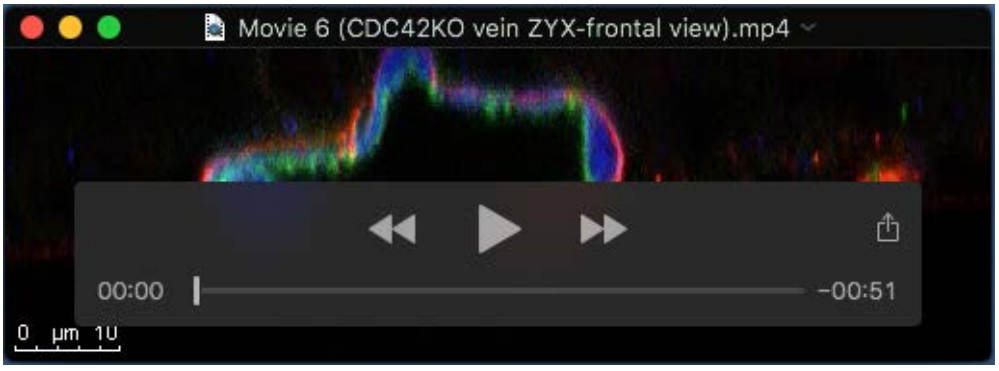

Movie 6

Movie 7

Movie 8

Movies 1-8: Animation of continuous optical ZYX (frontal view movies 1,2,5,6) and ZXY (lateral view movies 3,4,7,8) sections of arteries and veins from P7 control and *Cdc42*$^{\Delta EC}$ retinas. The abluminal (basal) surface of the endothelium is stained for Coll IV (red) while the luminal (apical) surface of the endothelium is identified by the ICAM2 staining (green). YFP expression indicates *Cdc42*KO-EC (pseudocolored in blue). Note that apical basal polarization and lumen formation in *Cdc42*$^{\Delta EC}$ arteries and veins appears normal but that veins are dilated.

1: ZYX (frontal) view of a control artery

2: ZYX (frontal) view of a *Cdc42*$^{\Delta EC}$ artery

3: ZXY (lateral) view of the control artery in S1

4: ZXY (lateral) view of the *Cdc42*$^{\Delta EC}$ artery in S2

5: ZYX (frontal) view of a control vein

6: ZYX (frontal) view of a *Cdc42*$^{\Delta EC}$ vein

7: ZXY (lateral) view of the control vein in S5

8: ZXY (lateral) view of the *Cdc42*$^{\Delta EC}$ vein in S6

Movie 9

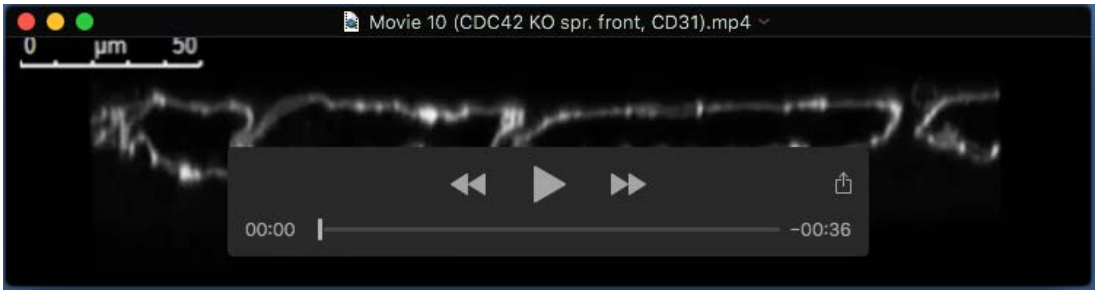

Movie 10

Movies 9, 10: Animation of continuous optical ZYX sections of blood vessels at the sprouting front (allowing a view into the vessel lumen) of P7 retinas. The image sequence is oriented proximal to distal with the first frame being located at more mature vessels of the sprouting front and the last frames ending with endothelial tip cells. Blood vessels stained with CD31 antibody (white). Vascular lumen of the sprouting front in control (**Movie 9**) and *Cdc42*$^{\Delta EC}$ retinas (**Movie 10**)

Movie 11: Capillary-venous malformations in *Cdc42*$^{\Delta EC}$ retinas

3-D reconstruction and subsequent animation of confocal sections from a P7 *Cdc42*$^{\Delta EC}$ retina stained with CD31. The confocal sections were acquired in the capillary network proximal to the sprouting front. Note the formation of large interconnected lumens in the cavernous like structures.

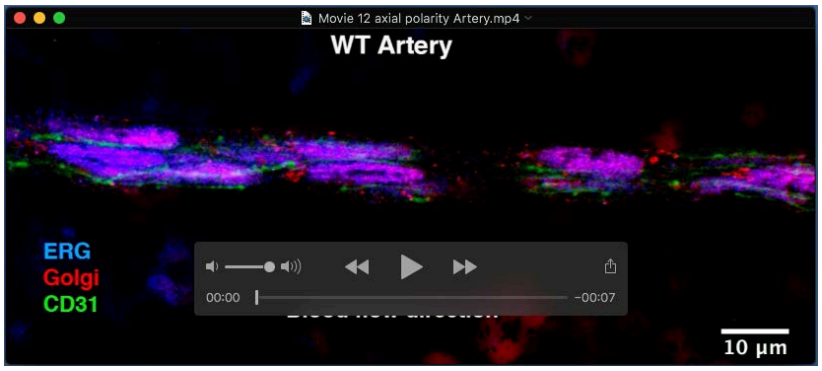

Movie 12: Evaluation of EC axial polarization *in-vivo*

Illustration of how EC polarization was quantified *in vivo* using individual sections of a z-stack. This example shows a representative control artery at P7. ERG (blue), CD31 (Green), and Golph4 (Red) stainings were combined to evaluate Golgi polarization. Confocal images were acquired at high magnification and the sequential z-slices from different channels were merged into a single hyperstack using FIJI software. Arterial ECs are highly polarized and orient their Golgi in front of the nucleus facing the predicted direction of blood flow (arrows).

Movie 13

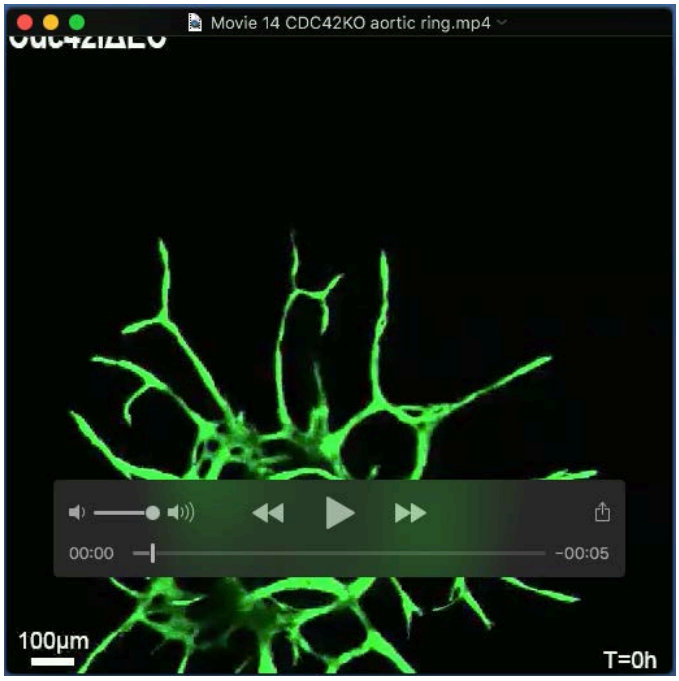

Movie 14

Movies 13,14: Time-lapse movies (47h) of Cldn5:GFP positive aortic rings from control **(Movie 13)** and *Cdc42*$^{\Delta EC}$ mice **(Movie 14)**.

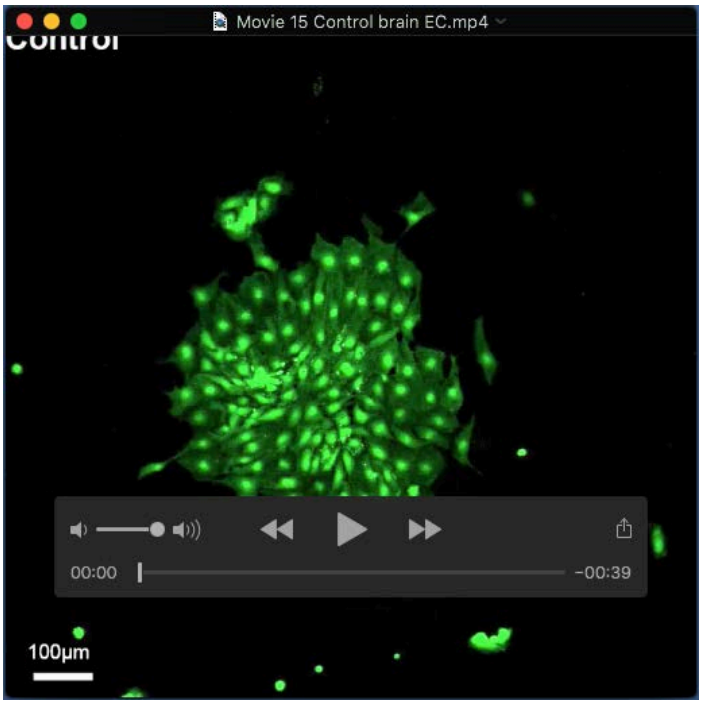

Movie 15

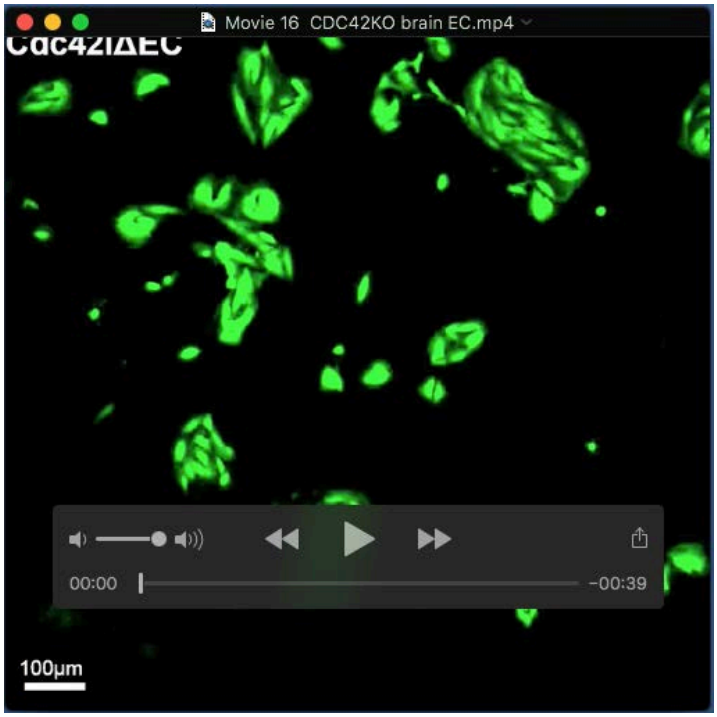

Movie 16

Movies 15, 16: Time-lapse movies (97h) of Cldn5:GFP positive primary brain EC clusters isolated from P7 control (**Movie 15**) and *Cdc42*^{iEC}(**Movie 16**) animals.

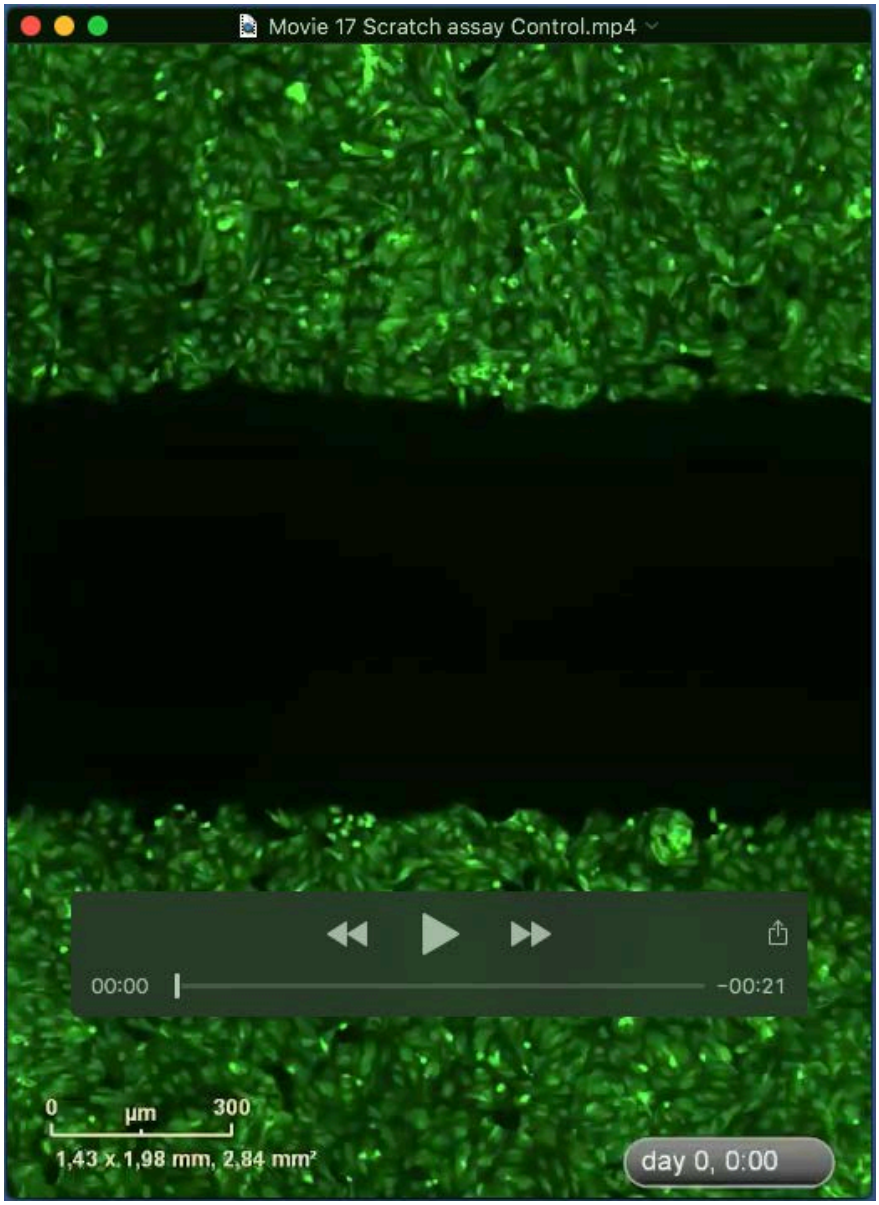

Movie 17

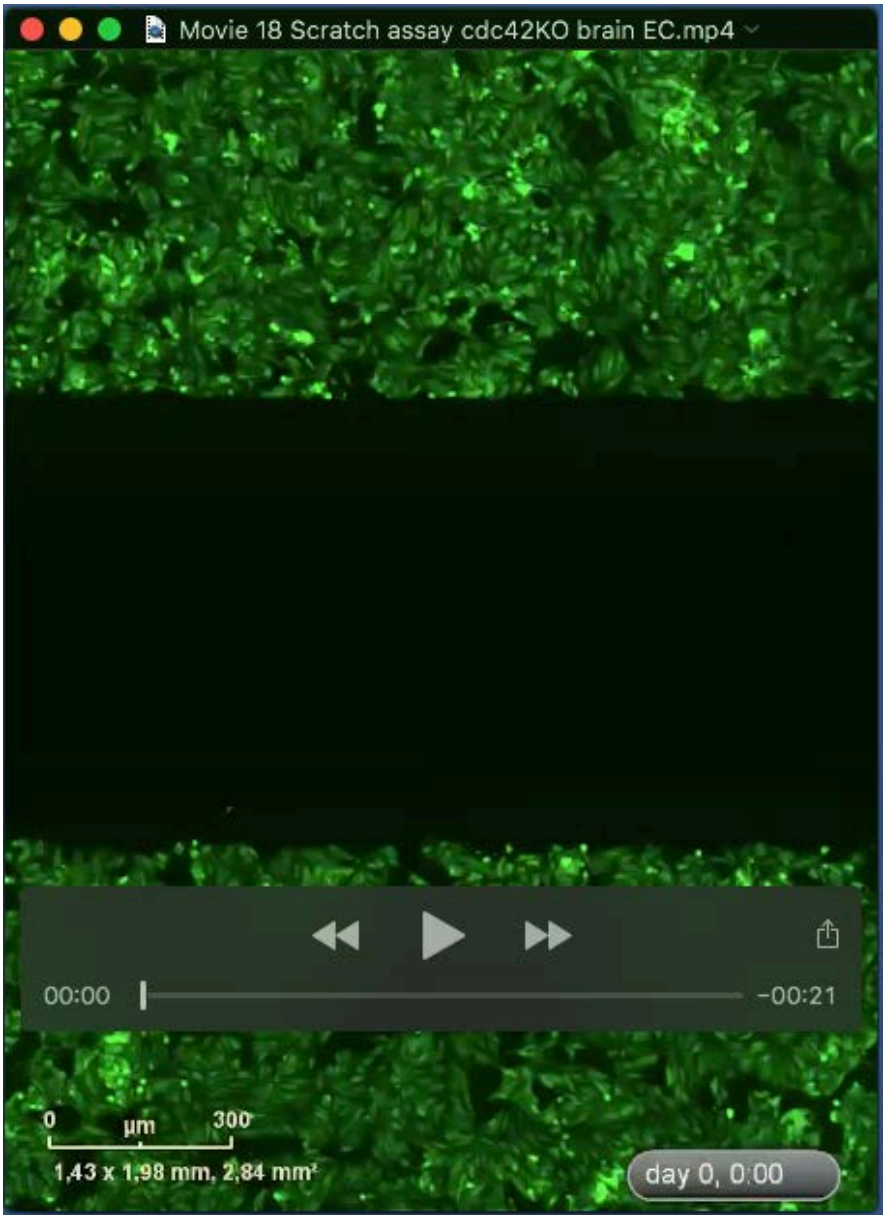

Movie 18

Movies 17, 18: Time-lapse movies (72h) of scratch assay from primary brain ECs (Cldn5:GFP positive) isolated from P7 control (**Movie 17**) and *Cdc42*$^{\Delta EC}$ (**Movie 18**) animals.

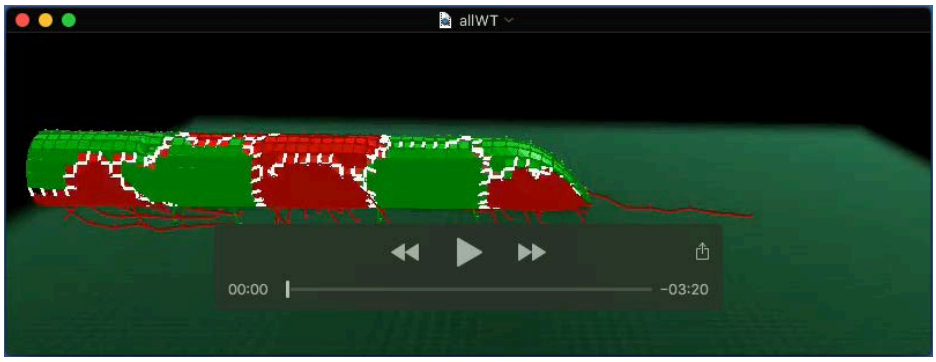

Movie 19: WT:WT sprout

Simulation movie showing a 1:1 WT:WT sprout in which both the green and red cells depict WT cells. The green and red cells are equally competent to occupy the tip position. The green layer underneath the vessel shows the VEGF gradient, which linearly increases towards the tip.

Movie 20: $Cdc42_{FIL}$:WT sprout

Simulation movie showing a 1:1 $Cdc42_{FIL}$:WT sprout in which the green and red cells respectively depict $Cdc42_{FIL}$ and WT cells. The green $Cdc42_{FIL}$ mutant cells extend less filopodia and are less competent to occupy the tip position than the red WT cells. The $Cdc42_{FIL}$ and WT cells segregate vertically, with the $Cdc42_{FIL}$ and WT cells respectively at the top and bottom of the vessel sprout, and this in a persistent way (compare with $Cdc42_{POL}$:WT sprout in Movie 22). They additionally segregate horizontally, with the $Cdc42_{FIL}$ cells at the rear of the sprout, albeit in a rather transient way (compare with $Cdc42_{POL}$:WT sprout in Movie 22). The green layer underneath the vessel shows the VEGF gradient, which linearly increases towards the tip.

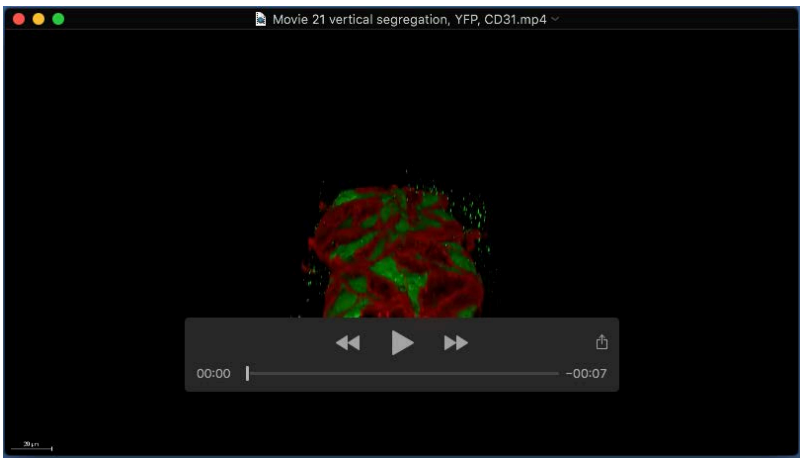

Movie 21: Vertical segregation of *Cdc42*KO-EC *in vivo*

Endothelial cells lacking Cdc42 preferentially occupy the upper side (facing the vitreous) of growing blood vessels and are underrepresented on the bottom side of vessels (facing the astrocytes). 3-D animation of a XYZ Confocal stack, showing a partially recombined vein in a P7 *Cdc42*$^{\Delta EC}$ retina. *Cdc42*KO cells are indicated by YFP expression (green), ECs are visualized by CD31 staining (red).

Movie 22: Cdc42$_{POL}$:WT sprout

Simulation movie showing a 1:1 Cdc42$_{POL}$:WT sprout in which the green and red cells respectively depict Cdc42$_{POL}$ and WT cells. The green Cdc42$_{POL}$ cells are less polarized and are less competent to occupy the tip position than the red WT cells. The Cdc42$_{POL}$ and WT cells segregate vertically, with the Cdc42$_{POL}$ and WT cells respectively at the top and bottom of the vessel sprout, albeit only transiently (compare with Cdc42$_{FIL}$:WT sprout in Movie 21). In contrast, the horizontal segregation of the Cdc42$_{POL}$ and WT cells, with the Cdc42$_{POL}$ cells at the rear of the sprout, occurs in a more persistent way (compare with Cdc42$_{FIL}$:WT sprout in Movie 21). The green layer underneath the vessel shows the VEGF gradient, which linearly increases towards the tip.

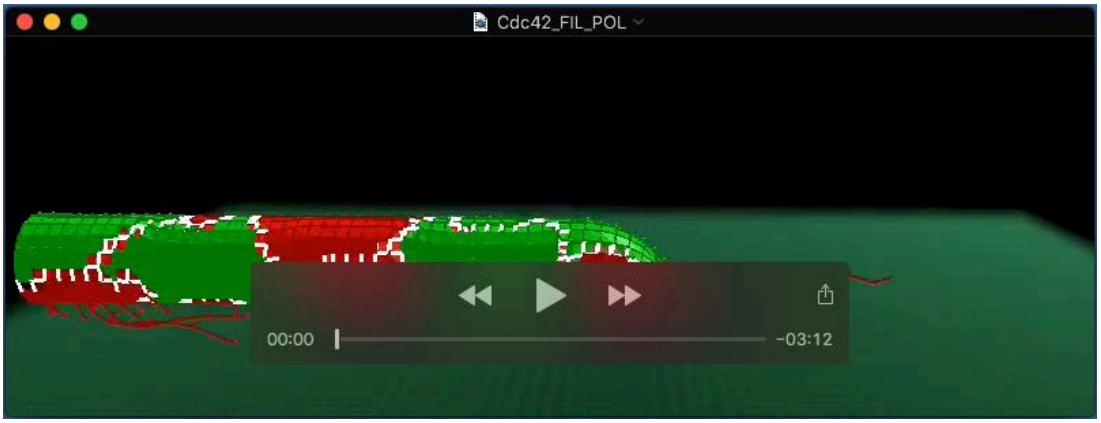

Movie 23: $Cdc42_{FIL/POL}$:WT sprout

Simulation movie showing a 1:1 $Cdc42_{FIL/POL}$:WT sprout in which the green and red cells respectively depict $Cdc42_{FIL/POL}$ and WT cells. The green $Cdc42_{FIL/POL}$ cells extend less filopodia, are less polarized and are less competent to occupy the tip position than the red WT cells. The $Cdc42_{FIL/POL}$ and WT cells both segregate vertically and horizontally. The green layer underneath the vessel shows the VEGF gradient, which linearly increases towards the tip.

Movie 24: $Cdc42_{COR}$:WT sprout

Simulation movie showing a 1:1 $Cdc42_{COR}$:WT sprout in which the green and red cells respectively depict $Cdc42_{COR}$ and WT cells. The green $Cdc42_{COR}$ cells extend less cortical protrusions and are less competent to occupy the tip position than the red WT cells. The $Cdc42_{COR}$ and WT cells thus segregate horizontally but not vertically. The green layer underneath the vessel shows the VEGF gradient, which linearly increases towards the tip.

Movie 25: $Cdc42_{ADH}$:WT sprout

Simulation movie showing a 1:1 $Cdc42_{ADH}$:WT sprout in which the green and red cells respectively depict $Cdc42_{ADH}$ and WT cells. The green $Cdc42_{ADH}$ cells are more strongly adhesive and consequently less motile which renders them less able to occupy the tip position than the red WT cells. The $Cdc42_{ADH}$ and WT cells thus segregate horizontally but not vertically. The green layer underneath the vessel shows the VEGF gradient, which linearly increases towards the tip.

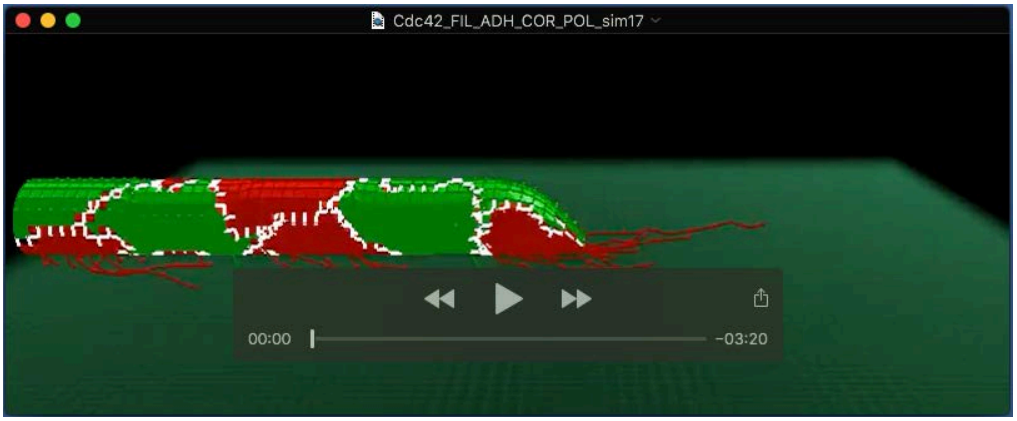

Movie 26: $Cdc42_{FIL/ADH/COR/POL}$:WT sprout

Simulation movie showing a 1:1 $Cdc42_{FIL/ADH/COR/POL}$:WT sprout in which the green and red cells respectively depict $Cdc42_{FIL/ADH/COR/POL}$ and WT cells. The green $Cdc42_{FIL/ADH/COR/POL}$ are less competent to occupy the tip position than the red WT cells. The $Cdc42_{FIL/ADH/COR/POL}$ and WT cells segregate both horizontally and vertically. The green layer underneath the vessel shows the VEGF gradient, which linearly increases towards the tip.